613. Sensitivity Analysis on Dynamic Responses of Geometrically Imperfect Base Excited Cantilevered Beams

O. Aghababaei, H. Nahvi*, S. Ziaei-Rad
Department of Mechanical Engineering, Isfahan University of Technology,
Isfahan 84156-83111, Iran
*Corresponding author. Tel: +98-311-3915242; Fax: +98-311-3912628
E-mail: *hnahvi@cc.iut.ac.ir*

(Received 25 November 2010; accepted 4 February 2011)

Abstract. The non-linear non-planar dynamic responses of a near-square cantilevered geometrically imperfect (i.e., slightly curved) beam under harmonic primary resonant base excitation with a one-to-one internal resonance is investigated. By assuming two different geometric imperfection shapes, the sensitivity of the perfect beam model predicted limit-cycles to small geometric imperfections is analyzed by continuing them versus the imperfection parameter incorporating the imperfect beam model. This was carried out by assuming that the corresponding frequency detuning parameter associated with each limit-cycle is fixed. Also, other possible branches of dynamic solutions for the corresponding fixed detuning parameter within the interval of the imperfection amplitude are determined and the importance of accounting for the small geometric imperfections is discussed.

Key words: Sensitivity analysis, Bifurcation, Limit-cycle, Chaos.

Nomenclature

m	- Mass per unit length of beam
D_{ii} , $i=\eta,\zeta$	- Flexural stiffness constants
$v(x,t), w(x,t)$	- Beam neutral axis deflection along *Y*, *Z* and *X* axes
$v_{\circ}(x), w_{\circ}(x)$	- Beam neutral axis natural deflection along *Y*, *Z* axes
c_i , $i=v,w$	- Damping coefficients
F	- Base excitation amplitude
Ω	- Excitation frequency
ω_{ni} , $i=z,y$	- Beam *n*th natural frequency along Z and Y axes
σ	- Excitation frequency detuning parameter
δ	- Beam cross section out-of-squareness detuning parameter
$\eta\zeta\xi$	- Current principle axes coordinate system of beam cross-section
XYZ	- Inertial reference coordinate system

1. Introduction

The non-linear dynamic response of a long, slender beam has been the subject of many theoretical and experimental efforts due to the fact that engineering structures like helicopter rotor blades, spacecraft antennae, flexible satellites, airplane wings, gun barrels, robot arms,

high-rise buildings, long-span bridges, and subsystems of more complex structures can be modeled as a beam-like slender member. Linear perfect (i.e. ignoring geometric imperfections) modeling of small-amplitude vibrating beams may contribute to results that match the experimental observations but when the amplitude of excitation is large, it does not predict the dynamic responses correctly. This is the consequence of ignoring several non-linearities such as inertia, curvature, mid-plane stretching, natural geometric imperfection and various beam effects like shear deformation, warping and rotary inertia. In the following survey, a brief summary of the most relevant works is presented.

Crespo da Silva and Glynn [1] investigated the flexural-flexural-torsional dynamics of beams to primary resonances accounting for both geometric and inertia non-linearities. They found that the first and the second mode response curves are different and response curves for higher modes are approximately independent of non-linear curvature terms. Whirling responses of near-square and near-circular cross-section beams to lateral base excitation, using the equations derived in [1] and ignoring the effect of damping, is investigated by Hyer [2]. He found that whirling motions exist near resonance excitation but could not locate unstable whirling motions. Crespo da Silva [3] used the same equations including damping and investigated the whirling motions of base-excited cantilever beams. He found that some whirling motions are unstable; furthermore, neither planar nor non-planar stable steady state motions existed in some ranges of frequency detuning. Crespo da Silva [4] investigated the planar response of an extensional beam to a periodic excitation. He found that the effect of the non-linearity due to mid-plane stretching is dominant and that neglecting the non-linearities due to curvature and inertia does not introduce significant error in the results. Also, unlike the response of an inextensional beam, the single-mode response of an extensional beam is always hardening. Pai and Nayfeh [5] investigated the non-planar oscillations of compact (i.e. near-square) beams under lateral base excitations. They located Hopf bifurcations and found that the system can exhibit quasi-periodic or chaotic motions; furthermore, the low-frequency modes are dominated by geometric non-linearities while the high-frequency modes are dominated by inertia non-linearities. Crespo da Silva and Zaretzky [6] studied the non-linear responses of compact cantilever and clamped-pinned/sliding beams in the presence of a one-to-three internal resonance. Zaretzky and Crespo da Silva [7] experimentally investigated the non-linear modal coupling in the response of compact cantilever beams and obtained good agreement with the theoretical predictions of ref. [6]. Crespo da Silva and Zaretzky [8] examined the flexural-torsional coupling in inextensional beams for a case of one-to-one internal resonance between an in-plane bending mode and a torsional mode and excited the in-plane mode. They found that within certain ranges of the excitation amplitude, the in-plane bending component of the coupled response saturates so that any further energy pumped into the system is transferred to the torsional motion via the internal resonance. Luczko [9] used a geometrically accurate model to investigate the bifurcations and internal resonances in extensional space-curved rods. The model includes non-linear expressions of strains as functions of generalized co-ordinates, non-linear material equations, as well as all non-linear terms in the equations of motion derived from the balance of momentum and angular momentum. He found a vast variety of internal resonance phenomena, which are caused by the coupling due to the inclusion of geometrical non-linearities. Avramov [10] investigated the non-linear oscillations of a simply supported beam subjected to a periodic force at a combination resonance. He used the center manifold method and discovered the Naimark–Sacker bifurcations leading to almost-periodic oscillations. Dwivedy and Kar [11] investigated the non-linear dynamics of a base-excited slender beam carrying a lumped mass subjected to simultaneous combination parametric resonance of sum and difference type along with 1:3:5 internal resonances. They observed interesting phenomena like blue sky catastrophe, jump down phenomena and simultaneous occurrence of periodic and chaotic orbits. Lacarbonar et al. [12] investigated non-linear interactions in a hinged–hinged uniform moderately curved beam with a torsional spring at one end. The beam mixed-mode

response is shown to undergo several bifurcations, including Hopf and homoclinic bifurcations, along with the phenomenon of frequency island generation and mode localization. Luongo and Egidio [13] applied the multiple scales method to a one-dimensional continuous model of planar, inextensible and shear-undeformable straight beam to derive the equations governing the system asymptotic dynamic around a bifurcation point. They studied the post-critical behavior around the bifurcations. Paolone et al. [14] analyzed the stability of a cantilever elastic beam with rectangular cross-section under the action of a follower tangential force and a bending conservative couple at the free end. The linear stability of the trivial equilibrium is studied, revealing the existence of buckling, flutter and double-zero critical points.

Aghababaei et al. [15] derived the non-linear equations and boundary conditions of non-planar (two bending and one torsional) vibrations of inextensional isotropic geometrically imperfect beams (i.e. slightly curved and twisted beams) using the extended Hamilton's principle. The order of magnitude of the natural geometric imperfection was assumed to be the same as the first order of vibrations amplitude. Although the natural imperfection is small, their study shows that in contrast to the case of straight beams (i.e. geometrically perfect beams), the vibration equations are linearly coupled and have linear and quadratic terms in addition to cubic terms. Also, in the case of near-square or near-circular beams, coupling terms between lateral and torsional vibrations exist. Furthermore, a problem of parametric excitation in the case of perfect beams changes to a problem of mixed parametric and external excitation in the case of imperfect beams. They have also investigated the validity of the proposed model using the existing experimental data.

Aghababaei et al. [16] investigated the non-linear non-planar steady-state responses of a near-square cantilevered beam (a special case of inextensional beams) with geometric imperfection under harmonic base excitation using the equations in [15]. By applying the combination of the multiple scales method and the Galerkin procedure to two non-linear integro-differential equations derived in [15], two modulation non-linear coupled first-order differential equations were obtained for the case of a primary resonance with a one-to-one internal resonance. They showed that the modulation equations contain linear imperfection-induced terms in addition to cubic geometric and inertial terms. Variations of the steady-state response amplitude curves with different parameters were presented. Bifurcation analyses of fixed points show that the influence of geometric imperfection on the steady-state responses can be significant to a great extent although the imperfection is small. The phenomenon of frequency island generation was also observed.

In this paper, by assuming two different geometric imperfection shapes, each limit-cycle of the perfect cantilever beam is continued versus the imperfection parameter (this is done by assuming that the corresponding frequency detuning parameter is fixed) and the sensitivity of the limit-cycle to small geometric imperfections is investigated. Also, other possible branches of dynamic solutions for the corresponding fixed detuning parameter within the interval of the imperfection amplitude are determined and the importance of taking into account the small geometric imperfections is discussed.

2. Problem Description and Equations

The same notations as in [16] are used to analyze the dynamic solutions in non-linear vibrations of an imperfect and perfect, cantilevered, base-excited beam with near-square cross-section, as shown in Fig. 1. It should be noted that for a perfect beam, the geometric imperfection (small initial non-dimensional deflection functions of the beam neutral axis, $v_{\circ}(x)$ and $w_{\circ}(x)$), as shown in Fig. 1, are zero (i.e. $v_{\circ}(x)=w_{\circ}(x)=0$). In this figure, XYZ and $\eta\zeta\xi$ denote the inertial and the cross-section principle coordinate systems, respectively.

In this paper, the primary-resonant excitation of the *n*th mode in the *Z*-direction (ω_{nz}), $\Omega = \omega_{nz}(1+\varepsilon^2\sigma)$, which in turn excites the *n*th mode in the *Y*-direction (ω_{ny}) through a one-to-one internal resonance $\omega_{ny} = \omega_{nz} \equiv \omega_n$ with zero external detuning is analyzed (σ is the frequency detuning parameter). There exists such an internal resonance for near-square beams. Since the former and later modes are excited directly by the primary resonance and indirectly through the one-to-one internal resonance, respectively, they are the only non-decaying contributing modes in the response of the beam [16]. It is assumed that none of the other modes in the *Y*- and *Z*-directions is involved in any internal resonance with the 2nd mode in the *Y*- or *Z*-direction.

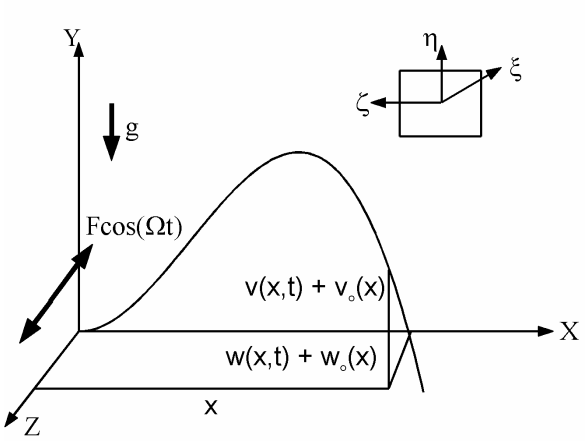

Fig. 1. Geometrically imperfect cantilever beam under base excitation, *XYZ*: inertial coordinate system, $\eta\zeta\xi$: principle axes of the beam cross-section (deflections are shown exaggeratedly)

Expanding the in-plane and out-of-plane non-dimensional deflection variables (i.e. *v*(*x*,*t*) and *w*(*x*,*t*), respectively) in power series involving a bookkeeping perturbation parameter ε as $\chi(x,t;\varepsilon) = \varepsilon\chi_1(x,T_\circ,T_2) + \varepsilon^3\chi_3(x,T_\circ,T_2) + \ldots$ where $\chi = v, w$ and $\chi_1(x,T_\circ,T_2) = X_n(x)a_{\chi n}(T_2)\cos\left[\omega_n T_\circ + \rho_{\chi n}(T_2)\right]$, $X_n(x)$ is the n*th* normalized flexural mode shape (i.e. single mode approximation of the response, it is assumed that the 2nd in-plane and out-of-plane flexural modes are interacting under the primary resonance $\Omega = \omega_n(1+\varepsilon^2\sigma)$) and $T_i = \varepsilon^i t$, $i = 0, 2$, the following modulation equations are obtained (for the sake of briefness, the modulation equations are directly adopted, for a detailed perturbation analysis, the reader is referred to [16]):

$$-2\omega_n p_{vc}' = (C_4 + C_9)p_{vs} - C_1 p_{vc} + C_3 p_{ws} - C_5\left[(p_{vc}^2 + p_{vs}^2)p_{vs} - 2p_{vc}^2 p_{vs}\right] + (C_6 - C_2)\left[p_{vs}(p_{wc}^2 + p_{ws}^2)\right] + 2C_2 p_{vc} p_{wc} p_{ws} \quad (1a)$$

$$-2\omega_n p_{vs}' = -(C_4 + C_9)p_{vc} - C_1 p_{vs} - C_3 p_{wc} - C_5\left[(p_{vc}^2 + p_{vs}^2)p_{vc} + 2p_{vc} p_{vs}^2\right] - 2C_2 p_{vs} p_{wc} p_{ws} - (C_2 + C_6)\left[(p_{wc}^2 + p_{ws}^2)p_{vc}\right] \quad (1b)$$

$$-2\omega_n p'_{wc} = (C_8 + C_9)p_{ws} - C_1 p_{wc} + C_7 p_{vs} - C_5\left[(p_{wc}^2 + p_{ws}^2)p_{ws} - 2p_{wc}^2 p_{ws}\right] + 2C_2 p_{wc} p_{vc} p_{vs} + (C_6 - C_2)\left[(p_{vc}^2 + p_{vs}^2)p_{ws}\right] \quad (1c)$$

$$-2\omega_n p'_{ws} = -(C_8 + C_9)p_{wc} - C_1 p_{ws} - C_7 p_{vc} - C_5\left[(p_{wc}^2 + p_{ws}^2)p_{wc} + 2p_{wc} p_{ws}^2\right] - 2C_2 p_{ws} p_{vc} p_{vs} - (C_2 + C_6)\left[(p_{vc}^2 + p_{vs}^2)p_{wc}\right] - \alpha_{21} f\ \omega_n^2 \quad (1d)$$

where $p_{ic} = a_{in}\cos\gamma_{in}$, $p_{is} = a_{in}\sin\gamma_{in}$ and $\gamma_{in} = \omega_n \sigma T_2 - \rho_{in}$, $i = v, w$.

In the above equations, f denotes the scaled non-dimensional amplitude of base excitation (i.e. $\varepsilon^3 f = F$), $\alpha_{21} = \int_0^1 X_n dx$ and C_1 to C_9 are defined in the Appendix II of ref. [16]. It should be noted that the ratio $D_{\zeta\zeta}/D_{\eta\eta}$ is ordered to $1+\varepsilon^2\delta$ for near-square beams where δ denotes the out-of-squareness of beam cross-section and appears in the constant C_4. The damping factors in both directions are assumed to be equal $d_w = d_v = d$ and ordered to $\varepsilon^2\mu$ which appears in the constant C_1. The effect of geometric imperfection appears in the constants $C_3, C_4, C_7,$ and C_8.

In Section 3, Eqs. (1a)-(1d) are applied to determine the limit-cycles in non-linear non-planar (bending-bending) vibrations of an imperfect base-excited cantilever beams with the primary resonant excitation of the second flexural mode in the *Z*-direction (i.e. ω_{2z}), which in turn excites the second flexural mode in the *Y*-direction (i.e. ω_{2y}) through a one-to-one internal resonance $\omega_{2y} = \omega_{2z} \equiv \omega_2$. For the sake of simplicity, a_χ, ρ_χ, and ω are used instead of $a_{\chi 2}$, $\rho_{\chi 2}$, and ω_2, $\chi = v, w$, respectively.

3. Imperfect Beam Limit-Cycles

Among the methods of constructing limit-cycles such as brute-force approach [17], harmonic balance method [18] and time-domain methods [19], it was decided to use the brute-force method. In this method, one chooses an initial condition, integrates the system of Eqs. (1a)-(1d) and ultimately converges to an attractor that may or may not be a limit-cycle. Since the frequency-domain and time-domain methods have their own restrictions to converge [17], the brute-force method was used for its convenient programming. Applying the Eqs. (1a)-(1d), invoking $v_\circ(x) = w_\circ(x) = 0$ (i.e. the perfect beam), and using the brute-force method, it was possible to determine twelve distinct limit-cycles for the perfect beam.

3.1. Sensitivity to Small Geometric Imperfections

In this section, the effect of small geometric imperfections on the dynamic response of the perfect beam is analyzed by assuming two different sample imperfection shapes

$$v_\circ(x) = c\left(X_1(x) + X_2(x)\right),\ w_\circ(x) = 0, \quad (2a)$$

$$v_\circ(x) = 0,\ w_\circ(x) = c\left(X_1(x) + X_2(x)\right). \quad (2b)$$

Note that in Eqs. (2a) and (2b), $X_1(x)$ and $X_2(x)$ are the first and second mode shapes of natural undamped vibrations of the perfect beam, respectively. The imperfection shapes in Eqs. (2a) and (2b) resemble a slightly arched cantilever beam in *XY* and *XZ* planes, respectively. Also, it is possible to determine different limit-cycles for the fixed frequency detunings within the imperfection amplitude (i.e. *c*) interval of (0-0.001) for the two imperfection shapes in Eqs. (2a) and (2b), which are not shown here. The branches of periodic solutions for the two imperfection cases in Eqs. (2a) and (2b) are computed by continuation of the perfect beam limit-cycles using the Auto 2000 [20] continuation software.

3.1.1. Sensitivity analysis of the 1st limit-cycle

As Fig. 2 shows, the perfect beam model predicts a limit-cycle at $\sigma = -0.011249$ and $c = 0$. By introducing an imperfection of the shape defined in Eq. (2a) into the perfect beam, applying the imperfect beam model modulation Eqs. (1a)-(1d) and continuing the predicted limit-cycle versus the imperfection amplitude *c* from zero, one arrives at a stable branch of periodic solutions that is terminated by a supercritical Hopf-bifurcation at $c_{HF} = 1.64678 \times 10^{-4}$ (see Fig. 2a). The post-bifurcation state is attracted by stable steady state non-planar vibrations. At the imperfection amplitude $c = 7.0034 \times 10^{-4}$, the system state jumps to steady state planar vibrations (*XZ*) since the system poses a saddle-node bifurcation at the specified imperfection amplitude.

Fig. 2b shows the branches of periodic solutions and chaotic bands for the imperfection shape defined in Eq. (2b). In this case, by continuing the perfect beam model predicted limit-cycle at $\sigma = -0.011249$, a stable branch of periodic solutions is obtained which undergoes a period-doubling bifurcation. Continuation of the period-doubled stable branch (not shown) reveals the existence of another period-doubling bifurcation. The sequence of period-doubling bifurcations persists which culminates in chaos.

Another branch of periodic solutions is obtained by forward and backward continuation of the limit-cycle shown in Fig. 3 for $c = 0.00061$ in Fig. 2b. When $c = 6.1935 \times 10^{-4} \equiv c_{HB}$, the limit-cycles become homoclinic to the saddle-focus $(p_{vc}, p_{vs}, p_{wc}, p_{ws}) = (0, 0, 0.0158123, 0.0117225)$. This is confirmed by the fact that the period of limit-cycle approaches infinity as *c* reaches the c_{HB}.

As discussed in [16], the coefficient C_3 in Eqs. (1a) and (1b) is zero for the perfect beam and also for both the imperfection cases defined in Eqs. (2a) and (2b). Thus, care should be taken that the modulation Eqs. (1a) - (1d) poses the symmetry $(p_{vc}, p_{vs}, p_{wc}, p_{ws}) \Leftrightarrow (-p_{vc}, -p_{vs}, p_{wc}, p_{ws})$. This indicates that for any asymmetric limit-cycle of the perfect and imperfect beams discussed in this paper, another limit-cycle may be obtained by reversing the signs of p_{vc} and p_{vs} state variables. Here, by saying the limit-cycles becoming homoclinic to saddle-focus it means that the two asymmetric limit-cycles (one of them obtained by the above-mentioned method) come close to each other as *c* approaches c_{HB} from the left until they meet at the saddle-focus, become merged, and form a single symmetric limit-cycle after homoclinic bifurcation.

The asymmetric branch of periodic solutions before homoclinic bifurcation changes to a symmetric branch after the homoclinic bifurcation. The symmetric branch undergoes two cyclic-fold bifurcations and then loses symmetry through a symmetry-braking bifurcation. A stable asymmetric branch emanates from the symmetry-braking bifurcation. Finally, a sequence of period-doubling bifurcations occurs culminating in chaos. The chaotic motion transits to steady state planar (*XZ* plane) motion through a boundary crisis at about $c = 6.7 \times 10^{-4}$.

It is interesting to note that for imperfection amplitudes greater than $c = 6.7\times10^{-4}$, the out-of-plane vibrations are suppressed. In other words, modal interaction between the primary resonantly excited mode (i.e. the second flexural mode) in *XZ* plane (see Fig. 1) and the second out-of-plane flexural mode in *XY* plane through an internal resonance is canceled.

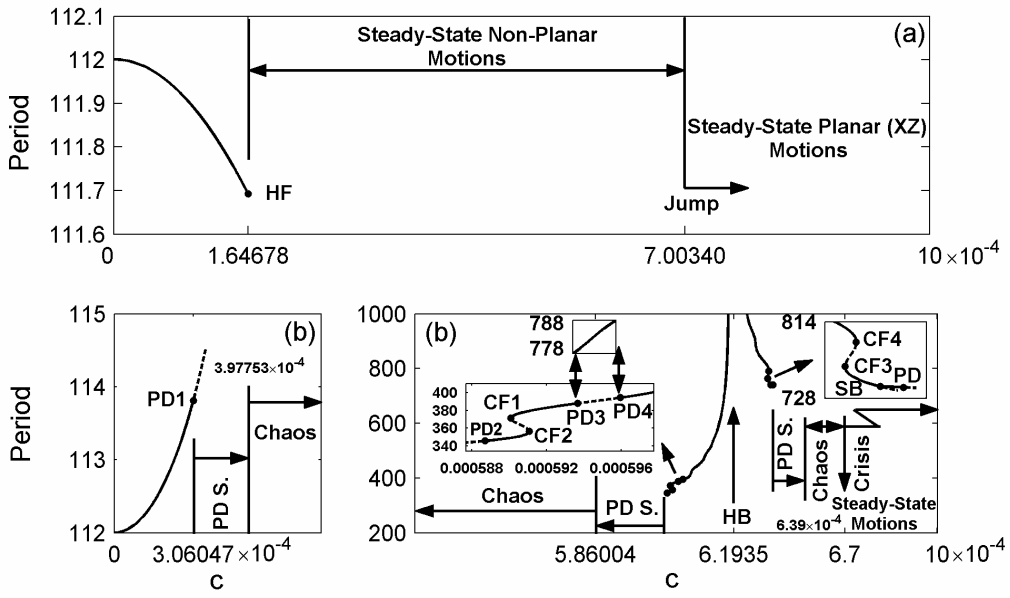

Fig. 2. Branches of periodic solutions and the chaotic bands when $\sigma = -0.011249$, $\mu = 0.04$, $\delta = 0.002$, $\alpha_{21} f = 6\times10^{-5}$ for two geometric imperfection shapes, (——) stable, (-----) unstable, HF, Hopf-bifurcation; PD, Period-Doubling; PD S., Period-Doubling Sequence; CF, Cyclic-Fold; HB, Homoclinic Bifurcation (a) $v_\circ(x) = c\left(X_1(x) + X_2(x)\right), w_\circ(x) = 0$, (b) $w_\circ(x) = c\left(X_1(x) + X_2(x)\right), v_\circ(x) = 0$

Fig. 3 shows dynamic responses for six sample imperfection amplitudes *c* and $\sigma = -0.011249$. The presence of sub-harmonic of order $\frac{1}{2}$ in the second FFT ($c = 0.00039$) in Fig. 3 is a characteristic of period-two limit-cycle, i.e. the period of the limit-cycle is doubled with respect to the period before period-doubling bifurcation. The fifth FFT ($c = 0.00062$) in Fig. 3 contains only odd harmonics which certifies the symmetry of its corresponding limit-cycle. The broadband nature in the third and sixth FFTs is the characteristic of chaotic motions.

3.1.2. Sensitivity analysis of the 2nd limit-cycle

Fig. 4 shows the branches of periodic solutions and chaotic bands that may appear for $\sigma = -0.01105$ with values of imperfection amplitude up to $c = 0.001$.

Fig. 4a reveals the extent of sensitivity of the perfect beam model predicted limit-cycle to small geometric imperfections of the shape defined in Eq. (2a) since the period of limit-cycle tends to infinity as $c \to 1.10147\times10^{-4}$. The imperfect beam model poses a saddle-focus at $c = 1.10147\times10^{-4} \equiv c_{HB}$ and the limit-cycles experience a homoclinic bifurcation when $c = c_{HB}$. The symmetric limit-cycle changes to an asymmetric one after homoclinic bifurcation.

The period decreases for imperfection amplitudes larger than c_{HB} and the branch of periodic solutions undergoes a number of cyclic-fold and period-doubling bifurcations. For values larger than c_{CF3}, the system response is chaotic. The chaotic band is followed by periodic motions that their period decreases through an infinite number of reverse period-doubling bifurcations until the system state is attracted by the last period-one branch of periodic solutions. The last branch is terminated by a super-critical Hopf-bifurcation at $c = 7.57904 \times 10^{-4}$. The post-bifurcation state is attracted by steady state non-planar vibrations. At the imperfection amplitude $c = 9.9781 \times 10^{-4}$, the system state jumps to steady state planar vibrations (*XZ*) since the system poses a saddle-node bifurcation at the specified imperfection amplitude.

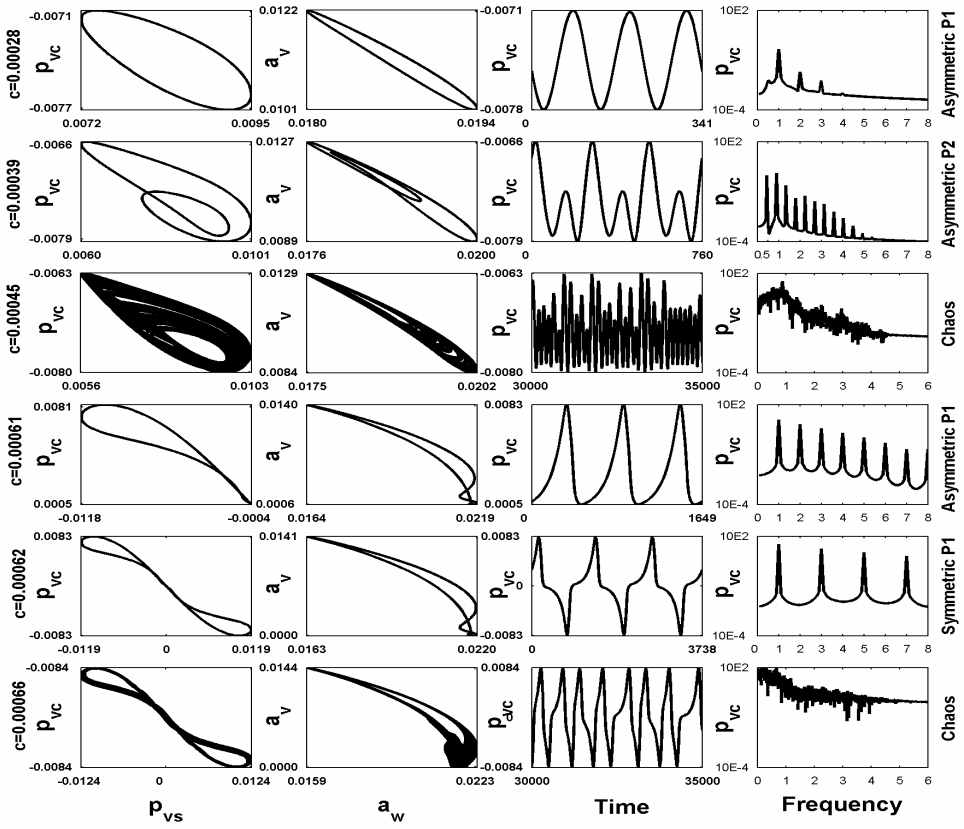

Fig. 3. The phase portraits, time traces, and FFTs of the limit-cycles depicted from the branches in Fig. 2 for the imperfect beam model with $w_\circ(x) = c\big(X_1(x) + X_2(x)\big), v_\circ(x) = 0$ when $\sigma = -0.011249$, $\mu = 0.04$, $\delta = 0.002$, $\alpha_{21} f = 6 \times 10^{-5}$

As Fig. 4b shows, the period of limit-cycle decreases considerably by increasing the imperfection amplitude from zero. After passing through two cyclic-fold bifurcations, the stable branch of symmetric periodic solutions loses symmetry through a symmetry-braking bifurcation. A stable branch of asymmetric periodic solutions emanates from the later bifurcation, undergoes four period-doubling bifurcations that results in stable period-doubled branches of periodic solutions, and finally ends at the symmetry-braking bifurcation SB2. The unstable part of a branch of symmetric periodic solutions that passes through the SB2 is not

clear in Fig. 4b. The stable part (to the right of SB2) undergoes two cyclic-fold bifurcations and loses its symmetry through SB3. A stable branch of asymmetric periodic solutions emerges from SB3 and goes through PD5, PD6, and CF5. An infinite number of period-doubling bifurcations occur after and before PD5 and PD6, respectively, culminating in chaos.

Care should be taken that the previous branches of periodic solutions are located within $c = 0$ and $c = 2.05089 \times 10^{-4}$. As Fig. 4b indicates, for certain ranges of *c*, more than one periodic solution exists. For the values of imperfection amplitude between c_{CF5} and c_{CF6} the dynamic response is chaotic. After the two remaining branches in Fig. 4b, chaotic motion is predicted. As shown in Fig. 4b, the chaotic motion transits to steady state planar motion through a boundary crisis at about $c = 2.60791 \times 10^{-4}$.

Comparing Figs. 2b and 4b, one finds that transition from non-planar chaotic motions to planar steady state motions occurs at different values of imperfection amplitudes. This indicates that the frequency detuning parameter may play an important role on the amount of sensitivity to geometric imperfections.

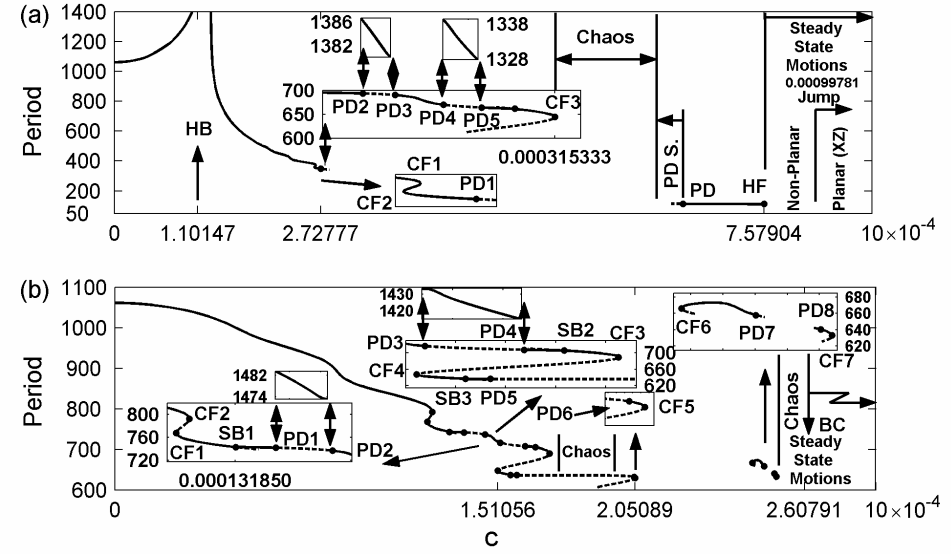

Fig. 4. Branches of periodic solutions and the chaotic bands when $\sigma = -0.01105$, $\mu = 0.04$, $\delta = 0.002$, $\alpha_{21} f = 6 \times 10^{-5}$ for two geometric imperfection shapes, (——) stable, (-----) unstable, HF, Hopf-bifurcation; PD, Period-Doubling; PD S., Period-Doubling Sequence; CF, Cyclic-Fold; HB, Homoclinic Bifurcation; BC, Boundary Crisis; SB, Symmetry-Braking (a) $v_\circ(x) = c\left(X_1(x) + X_2(x)\right), w_\circ(x) = 0$, (b) $w_\circ(x) = c\left(X_1(x) + X_2(x)\right), v_\circ(x) = 0$

3.1.3. Sensitivity analysis of the 3rd, 4th, and 5th limit-cycles

Figs. 5 and 6 represent the dynamic responses for the two imperfection cases that may appear for the frequency detunings $\sigma = -0.005169$ and $\sigma = -0.005161$, respectively.

In Fig. 5a, the periodic motions change to chaos through a cyclic-fold bifurcation as the imperfection amplitude increases beyond $c = 1.4996 \times 10^{-4}$. In Fig. 5b, first the stable periodic motions change to chaos through a cyclic-fold bifurcation at $c = 3.09386 \times 10^{-4}$, then,

the chaotic motions change to another symmetric periodic motion through a cyclic-fold bifurcation at $c = 3.16291 \times 10^{-4}$.

In Fig. 6a and 6b, first the branches of symmetric periodic solutions loses symmetry through symmetry-braking bifurcations, then, the stable branches of asymmetric periodic solutions emanating from the SBs experience period-doubling and cyclic-fold bifurcations, respectively. In Fig. 6a, a sequence of PDs occurs culminating in chaos while in Fig. 8b, transition to chaos occurs through the CF bifurcation.

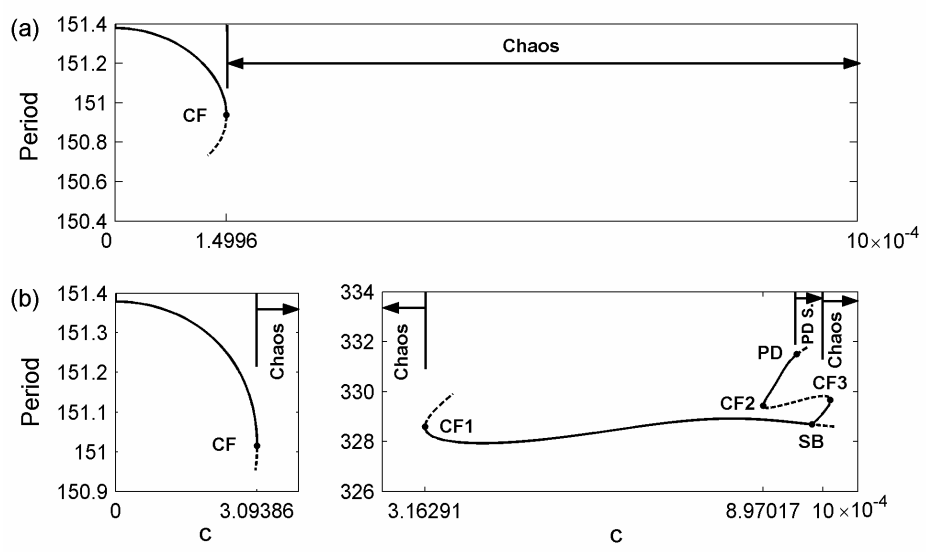

Fig. 5. Branches of periodic solutions and the chaotic bands when $\sigma = -0.005169$, $\mu = 0.04$, $\delta = 0.002$, $\alpha_{21} f = 6 \times 10^{-5}$ for two geometric imperfection shapes, (——) stable, (-----) unstable, PD, Period-Doubling; PD S., Period-Doubling Sequence; CF, Cyclic-Fold; SB, Symmetry-Braking (a) $v_\circ(x) = c\left(X_1(x) + X_2(x)\right), w_\circ(x) = 0$, (b) $w_\circ(x) = c\left(X_1(x) + X_2(x)\right), v_\circ(x) = 0$

Fig. 7a indicates the least sensitivity to geometric imperfections of the shape defined in Eq. (2a). Fig. 7b shows a scenario similar to that in Fig. 6a except that the bifurcations occur at different values of *c*.

3.1.4. Sensitivity analysis of the 7th and 8th limit-cycles

Parts (a) and (b) in Fig. 8 present the branches of periodic solutions and the chaotic bands predicted by the imperfect beam model for the imperfection shape defined in Eq. (2a) and the frequency detunings $\sigma = -0.002938$ and $\sigma = -0.001865$, respectively. The results for the imperfection shape defined in Eq. (2b) are not shown since they are similar to their counterparts except that the bifurcations occur at slightly different values of imperfection amplitude *c*. As Fig. 8 represents, by a slight increase in the imperfection amplitude *c*, the predicted limit-cycles by the perfect beam model change to limit-cycles with periods of one-half and one-fourth the corresponding perfect beam limit-cycles periods. In Fig. 8a, the branch of asymmetric period-one-fourth periodic solutions undergoes two recurrent cyclic-folds and ends at a symmetry-braking bifurcation. A branch of symmetric periodic solutions passes through the SB

bifurcation and continues up to $c = 0.001$. In Fig. 8b, the branch of asymmetric period-one-fourth periodic solutions ends at a SB bifurcation. A branch of symmetric periodic solutions goes through the SB bifurcation while loses stability through a CF bifurcation. For the imperfection amplitudes between c_{CF} and $c = 0.001$, chaotic motion is predicted.

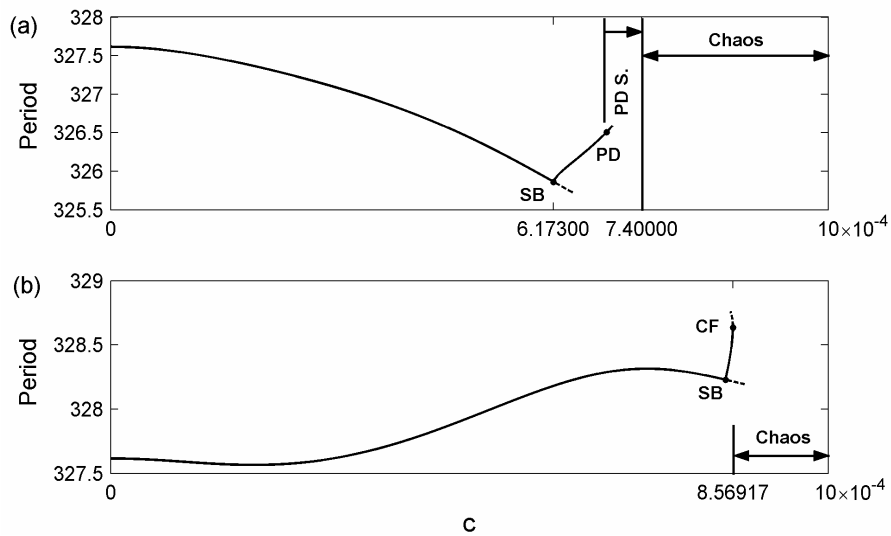

Fig. 6. Branches of periodic solutions and the chaotic bands when $\sigma = -0.005161$, $\mu = 0.04$, $\delta = 0.002$, $\alpha_{21} f = 6\times10^{-5}$ for two geometric imperfection shapes, (——) stable, (-----) unstable, PD, Period-Doubling; PD S., Period-Doubling Sequence; CF, Cyclic-Fold; SB, Symmetry-Braking (a) $v_\circ(x) = c\left(X_1(x) + X_2(x)\right), w_\circ(x) = 0$, (b) $w_\circ(x) = c\left(X_1(x) + X_2(x)\right), v_\circ(x) = 0$

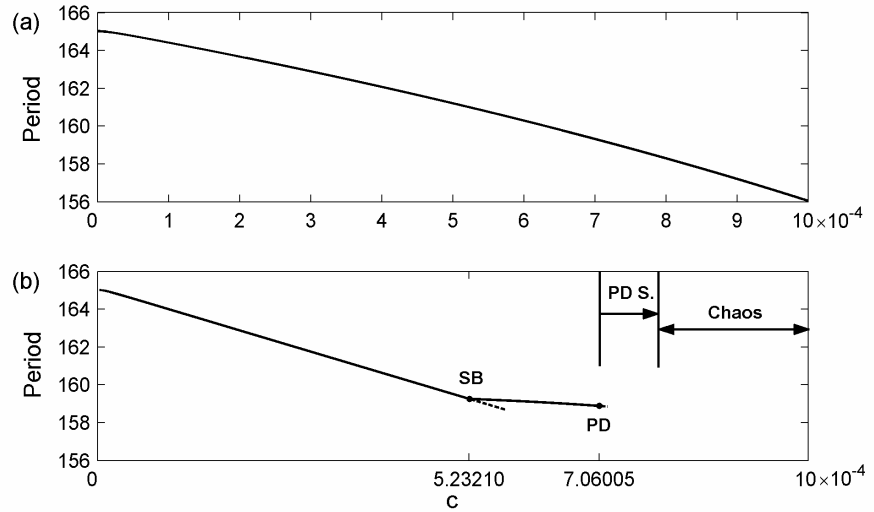

Fig. 7. Branches of periodic solutions and the chaotic bands when $\sigma = -0.004826$, $\mu = 0.04$, $\delta = 0.002$, $\alpha_{21} f = 6\times10^{-5}$ for two geometric imperfection shapes, (——) stable, (-----) unstable, PD, Period-Doubling; PD S., Period-Doubling Sequence; SB, Symmetry-Braking (a) $v_\circ(x) = c\left(X_1(x) + X_2(x)\right), w_\circ(x) = 0$, (b) $w_\circ(x) = c\left(X_1(x) + X_2(x)\right), v_\circ(x) = 0$

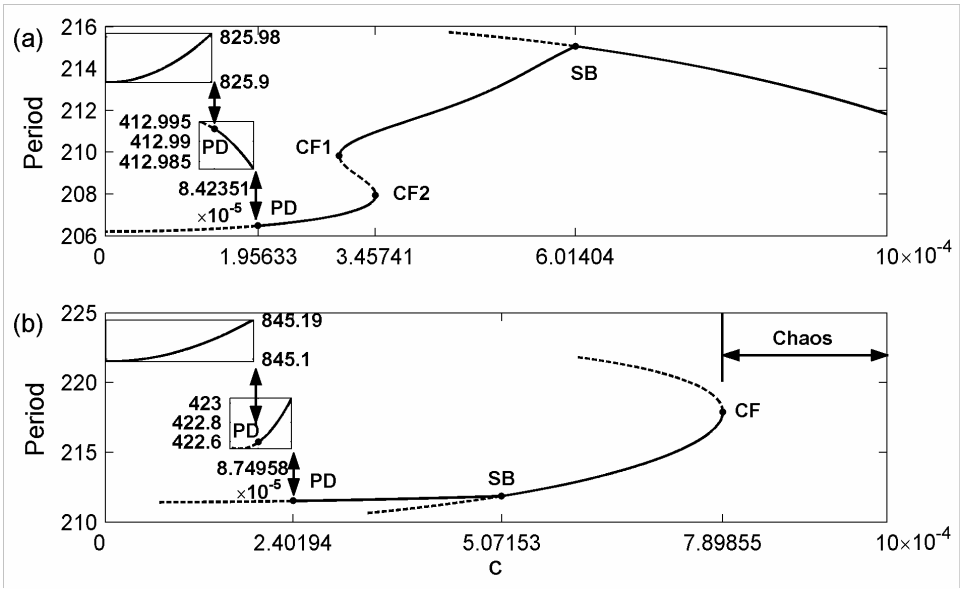

Fig. 8. Branches of periodic solutions and the chaotic bands when $\mu = 0.04$, $\delta = 0.002$, $\alpha_{21} f = 6\times10^{-5}$ for the geometric imperfection shape $v_\circ(x) = c\left(X_1(x) + X_2(x)\right), w_\circ(x) = 0$, (——) stable, (-----) unstable, PD, Period-Doubling; SB, Symmetry-Braking; CF, Cyclic-Fold, (a) $\sigma = -0.002938$, (b) $\sigma = -0.001865$

3.1.5. Sensitivity analysis of the 6th, 9th, 10th, 11th, and 12th limit-cycles

The continuation of the sixth, ninth, tenth, eleventh, and twelfth limit-cycles of the perfect beam should be found in Fig. 9. The imperfection shape in Fig. 9 is assumed to be the shape defined in Eq. (2a). For the sake of brevity, the continuation results for the imperfection shape defined in Eq. (2b) are not shown since they are similar to their counterparts in Fig. 9 except that the bifurcations occur at slightly different values of imperfection amplitude *c*.

The most sensitivity to small geometric imperfections is observed in parts (a) and (c) of Fig. 9. In part (a), for values of imperfection amplitude greater than $c = 2.36688\times10^{-4}$, the response would be chaotic instead of periodic. In part (b) of Fig. 9, the response is predicted to be period-*n* ($n = 1, 2, 3, \ldots$) or chaotic depending on the amplitude of the imperfection. The upper and lower branches in part (c) of Fig. 9 are obtained by continuation of the eleventh and tenth limit-cycles of the perfect beam, respectively, versus the imperfection amplitude. As Fig. 9c indicates, the tenth limit-cycle predicted by the perfect beam may be drastically affected by a small imperfection, i.e. period-one limit-cycles are predicted instead of the period-two limit-cycles for imperfection amplitudes greater than $c = 1.90820\times10^{-4}$. For imperfection amplitudes less than c_{CF1}, the system response may be attracted by any of the limit-cycles corresponding to the branches shown in Fig. 9c. Also, for imperfection values greater than c_{CF1} and less than c_{BC} in the upper branch, the response may be chaotic or periodic. The response is predicted to be periodic of one single shape (lower branch) for imperfection amplitudes greater than c_{BC} and less than $c = 0.001$.

Part (d) of Fig. 9 shows that the system poses a Hopf-bifurcation at $c_{HF} = 4.11610 \times 10^{-4}$. For $c > c_{HF}$, steady-state non-planar motion is predicted instead of the twelfth period-one limit-cycle of the perfect beam.

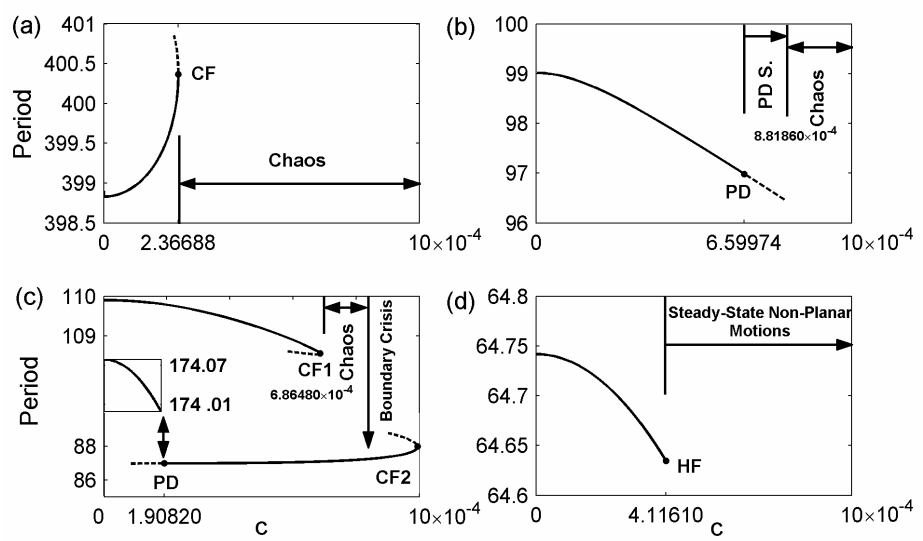

Fig. 9. Branches of periodic solutions and the chaotic bands when $\mu = 0.04$, $\delta = 0.002$, $\alpha_{21} f = 6 \times 10^{-5}$ for the geometric imperfection shape $v_\circ(x) = c\left(X_1(x) + X_2(x)\right), w_\circ(x) = 0$, (——) stable, (-----) unstable, PD, Period-Doubling; PD S., Period-Doubling Bifurcation; CF, Cyclic-Fold; HF, Hopf-Bifurcation, (a) $\sigma = -0.003285$, (b) $\sigma = -0.001618$, (c) $\sigma = -0.000975$, (d) $\sigma = -0.001$

Actually, one finds the importance of taking into account the geometric imperfection by considering the predicted possible dynamic responses of the imperfect beam model in Figs. 2 and 4-9 and comparing them with the perfect beam model predicted limit-cycles. These figures show that presence of small geometric imperfections in a near square cantilevered beam may lead to unexpected and completely different dynamic responses with respect to those predicted by the perfect beam model.

4. Conclusions

Investigation of the effect of small geometric imperfections on the dynamic response of cantilevered near-square beams should be conducted based on two points of view. First is the extent to which the geometric imperfection may affect a predicted periodic response by the perfect beam model and the second, is the comparison of branches of periodic solutions obtained by continuation of similar limit-cycles predicted by the perfect and imperfect beam models. Depending on the frequency detuning parameter, the sensitivity of the predicted limit-cycles by the perfect beam model to small geometric imperfections may be to a great extent, thus, ignoring the small geometric imperfections and applying the perfect beam model, may result in completely different and unexpected results.

References

[1] Crespo da Silva M.R.M., Glynn C.C. Nonlinear flexural-flexural-torsional dynamics of inextensional beams, II: Forced motions. J. Struct. Mech. 6**,** 449 (1978).
[2] Hyer M.W. Whirling of a base-excited cantilever beam. J. Acoust. Soc. Am. 65, 931 (1979).
[3] Crespo da Silva M.R.M. On the whirling of a base-excited cantilever beam. J. Acoust. Soc. Am. 67, 704 (1980).
[4] Crespo da Silva M.R.M. Non-linear flexural-flexural-torsional-extensional dynamics of beams, II: Response analysis. Int. J. Solids Struct. 24**,** 1235 (1988).
[5] Pai P.F., Nayfeh A.H. Non-linear non-planar oscillations of a cantilever beam under lateral base excitations. Int. J. Non-Linear Mech. 25, 455 (1990).
[6] Crespo da Silva M.R.M., Zaretzky C.L. Non-linear modal coupling in planar and non-planar responses of inextensional beams. Int. J. Non-Linear Mech. 25, 227 (1990).
[7] Zaretzky C.L., Crespo da Silva, M.R.M. Experimental investigation of non-linear modal coupling in the response of cantilever beams. J. Sound Vib. 174, 145 (1994).
[8] Crespo da Silva M.R.M., Zaretzky C.L. Nonlinear flexural-flexural-torsional interactions in beams including the effect of torsional dynamics, I: Primary resonance. Nonlinear Dynamics. 5, 3 (1994).
[9] Luczko J. Bifurcations and internal resonances in space-curved rods. Comput. Methods Appl. Mech. Engrg. 191, 3271 (2002).
[10] Avramov K.V. Non-linear beam oscillations excited by lateral force at combination resonance. J. Sound Vib. 257(2), 337 (2002).
[11] Dwivedy S.K., Kar R.C. Simultaneous combination and 1:3:5 internal resonances in a parametrically excited beam-mass system. Int. J. Non-Linear Mech. 38, 585 (2003).
[12] Lacarbonar W., Arafat H.N., Nayfeh A.H. Non-linear interactions in imperfect beams at veering. Int. J. Non-Linear Mech. 40, 987 (2005).
[13] Luongo A., Di Egidio A. Divergence, Hopf and double-zero bifurcations of a non-linear planar beam. Comput. Struct. 84, 1596 (2006).
[14] Paolone A., Vasta M., Luongo A. Flexural-torsional bifurcations of a cantilever beam under potential and circulatory forces I: Non-linear model and stability analysis. Int. J. Non-Linear Mech. 41, 586 (2006).
[15] Aghababaei O., Nahvi H., Ziaei-Rad S. Non-linear non-planar vibrations of geometrically imperfect inextensional beams, Part I: Equations of motion and experimental validation, Int. J. Non-Linear Mech. 44, 146-159 (2009).
[16] Aghababaei O., Nahvi H., Ziaei-Rad S. Non-linear non-planar vibrations of geometrically imperfect inextensional beams. Part II: Bifurcation analysis under base excitations, Int. J. Non-Linear Mech. 44, 160-178 (2009).
[17] Nayfeh A.H., Balachandran B. Applied Nonlinear Dynamics. John Wiley & Sons, Inc (1995).
[18] Kim Y.B., Noah S.T. Stability and bifurcation analysis of oscillators with piecewise linear characteristics: A general approach. J. Appl. Mech. 58, 545-553, 281 (1991).
[19] Rinzel J., Miller R.N. Numerical calculation of stable and unstable periodic solutions to the Hodgkin-Huxley equations, Math. Bioscience. 49, 27 (1980).
[20] Doedel E.J. et al. Auto 2000: Continuation and bifurcation analysis software for ordinary differential equations. California Institute of Technology. Pasadena. California. USA (2001).